

# Characteristics of the Mott transition and electronic states of high-temperature cuprate superconductors from the perspective of the Hubbard model

**Masanori Kohno**

International Center for Materials Nanoarchitectonics (WPI-MANA), National Institute for Materials Science, Tsukuba 305-0044, Japan

E-mail: KOHNO.Masanori@nims.go.jp

August 2017

**Abstract.** A fundamental issue of the Mott transition is how electrons behaving as single particles carrying spin and charge in a metal change into those exhibiting separated spin and charge excitations (low-energy spin excitation and high-energy charge excitation) in a Mott insulator. This issue has attracted considerable attention particularly in relation to high-temperature cuprate superconductors, which exhibit electronic states near the Mott transition that are difficult to explain in conventional pictures. Here, from a new viewpoint of the Mott transition based on analyses of the Hubbard model, we review anomalous features observed in high-temperature cuprate superconductors near the Mott transition.

Submitted to: *Rep. Prog. Phys.*

## 1. Introduction

In crystals, electrons usually behave as single particles carrying spin  $\hbar/2$  and charge  $-e$  under a periodic potential of ions [1]. However, the situation is not necessarily so simple in strongly interacting electron systems, where electronic states are strongly affected by other electrons. An obvious example is a Mott insulator [2], which exhibits low-energy spin excitation and high-energy charge excitation: the spin and charge excitations are separated. Thus, as the electron density increases, the electronic state changes from a metallic state in the low-electron-density regime, where electrons behave as single particles, into a Mott insulating state, where spin and charge excitations are separated, because of strong interactions between electrons.

A natural question is how the electronic state changes. As long as we consider that electrons behave as single particles carrying spin and charge, the spin-charge separated excitations in a Mott insulator cannot be well described. Conversely, if we consider that the spin and charge degrees of freedom are decoupled, the single-particle behavior in a metal is not well explained. This issue of the Mott transition is related to difficulties in dealing with strong electronic correlations (quantum many-body effects), and its essence cannot be understood in terms of conventional order parameters for symmetry breaking; the Mott transition can occur without magnetic ordering or structural symmetry breaking.

Conventionally, the Mott transition has been considered in the following pictures [3].

- *Rigid-band picture.*—The Mott transition is like a metal-insulator transition of a band insulator: holes disappear from the band top as the electron density (or the chemical potential) increases toward the Mott transition (figure 1(a)). In this case, the carriers are holes. The volume enclosed by the Fermi surface is proportional to the number of holes, which decreases toward the Mott transition.
- *Electron-like quasiparticle picture.*—Because the Mott transition is caused by strong electronic correlations, the effective mass of electrons (quasiparticles) diverges toward the Mott transition; the bandwidth of the quasiparticle narrows and disappears (figure 1(b)). In this case, the carriers are

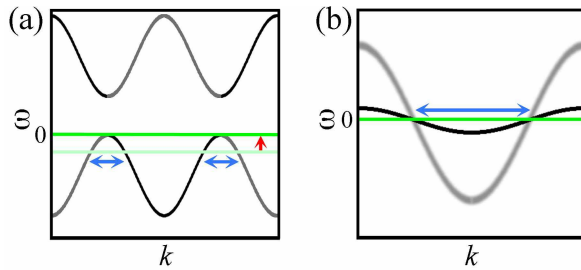


**Figure 1.** Conventional pictures of the Mott transition. (a) Schematic band structure (dispersion relation of single-particle excitation) in the rigid-band picture. As the chemical potential (green line) increases (red arrow), the volume of hole pockets (light-blue arrows) decreases. (b) Schematic band structure in the electron-like quasiparticle picture. As the effective mass increases, the bandwidth narrows (red arrows) with the volume inside the Fermi surface (light-blue arrow) remaining large.

the quasiparticles. The volume inside the Fermi surface is proportional to the number of electrons, which remains large even near the Mott transition.

Although these conventional pictures seem to explain some aspects of the Mott transition, some remarkable characteristics cannot be well understood in the conventional pictures. In particular, in high-temperature (high- $T_c$ ) cuprate superconductors, which are obtained by doping Mott insulators [4], anomalous electronic states have been observed [5–13]; the understanding of the electronic states near the Mott transition is considered key to revealing the mechanism of high- $T_c$  superconductivity [13–16].

In this paper, based on recent results for Hubbard-type models [17–25], we discuss the nature of the Mott transition and review the anomalous electronic states observed in high- $T_c$  cuprates from a new viewpoint of the Mott transition.

The Hubbard model is defined by the following Hamiltonian:

$$\mathcal{H} = -t \sum_{\langle i,j \rangle, \sigma} (c_{i,\sigma}^\dagger c_{j,\sigma} + \text{H.c.}) + U \sum_i n_{i,\uparrow} n_{i,\downarrow} - \mu \sum_{i,\sigma} n_{i,\sigma},$$

where  $\langle i, j \rangle$  indicates that  $i$  and  $j$  are nearest-neighbor sites. Here,  $c_{i,\sigma}$  and  $n_{i,\sigma}$  denote the annihilation and number operators, respectively, of an electron with spin  $\sigma (= \uparrow, \downarrow)$  at site  $i$ . Hereafter, we use units with  $\hbar = 1$ . The hole doping concentration is defined as  $\delta = 1 - n$ , where  $n$  denotes the electron density.

The ground state of this model at half-filling ( $\delta = 0$ ) is a Mott insulator if the Coulomb repulsion  $U$  is much larger than the hopping integral  $t (> 0)$ . In

the Mott insulator, each site is occupied essentially by one electron. Then, if one electron is added, one site is doubly occupied, which costs energy of the order of the Coulomb repulsion  $U$ : charge excitation has a large gap [26]. However, electrons at neighboring sites can exchange spins with a small energy of the order of  $J(=4t^2/U)$  through the second-order hopping process [27], which implies that there is a low-energy spin excitation. Thus, the Mott insulator exhibits separated spin and charge excitations: low-energy spin excitations of  $O(J)$  and high-energy charge excitations of  $O(U)$ .

To discuss how the electronic state changes when the Mott insulator is doped, we study the spectral function defined as follows:

$$A(\mathbf{k}, \omega) = \begin{cases} \frac{1}{2} \sum_{j,\sigma} |\langle j | c_{\mathbf{k},\sigma}^\dagger | \text{GS} \rangle|^2 \delta(\omega - \epsilon_j) & \text{for } \omega > 0, \\ \frac{1}{2} \sum_{j,\sigma} |\langle j | c_{\mathbf{k},\sigma} | \text{GS} \rangle|^2 \delta(\omega + \epsilon_j) & \text{for } \omega < 0, \end{cases}$$

where  $c_{\mathbf{k},\sigma}^\dagger$  denotes the creation operator of an electron with momentum  $\mathbf{k}$  and spin  $\sigma(=\uparrow, \downarrow)$ , and  $\epsilon_j$  denotes the excitation energy from the ground state |GS> to the eigenstate  $|j\rangle$ . The spectral function represents the probability that we can add (remove) an electron with momentum  $\mathbf{k}$  and energy  $|\omega|$  for  $\omega > 0$  ( $\omega < 0$ ). In the noninteracting case ( $U = 0$ ), because  $c_{\mathbf{k},\sigma}^\dagger | \text{GS} \rangle$  is an eigenstate,  $A(\mathbf{k}, \omega)$  shows a single curve, as shown in figure 1(b). The spectral function can also be expressed as

$$A(\mathbf{k}, \omega) = -\frac{1}{\pi} \text{Im}G(\mathbf{k}, \omega),$$

by using the retarded single-particle Green function  $G(\mathbf{k}, \omega)$  [3]. The spectral function can be observed in angle-resolved photoemission spectroscopy (ARPES) for  $\omega < 0$  and in inverse ARPES for  $\omega > 0$  [5].

## 2. Mott transition in the one-dimensional Hubbard model

If there is a general characteristic of the Mott transition, it should appear even in the simplest model. Hence, in this section, we consider the one-dimensional (1D) Hubbard model, for which exact solutions [17, 28–32] and accurate numerical results are available [17, 32].

At zero electron density ( $n = 0$ ), the spectral function  $A(k, \omega)$  exhibits a single mode because there are no other electrons. When the system contains more than one electron, spectral weights emerge at high energies, which form the upper Hubbard band (UHB). As the electron density increases, the spectral weight of the UHB increases, while that of the lower Hubbard band (LHB) decreases. The mode exhibiting a free-electron-like dispersion relation around the Fermi level continuously deforms, decreasing the spectral weight for  $\omega > 0$  in the LHB [17]. Immediately before the Mott transition, the spectral-weight distribution

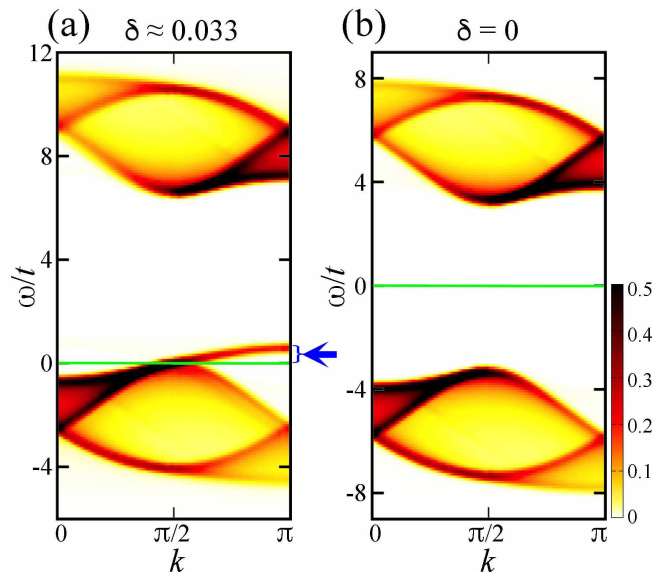


**Figure 2.** Spectral-weight distributions of the 1D Hubbard model for  $U/t = 10$  obtained using the non-Abelian dynamical density-matrix renormalization group (DDMRG) method on a 120-site chain with 120 density-matrix eigenstates [17, 21]. (a)  $A(k, \omega)t$  near the Mott transition ( $\delta \approx 0.033$ ). The blue arrow indicates the doping-induced states. (b)  $A(k, \omega)t$  of the Mott insulator ( $\delta = 0$ ). The green lines indicate the Fermi level ( $\omega = 0$ ). Gaussian broadening with a standard deviation of 0.1t is used.

becomes almost identical to that of the Mott insulator (figure 2(b)), except for the existence of the gapless dispersing mode for  $\omega > 0$  in the LHB (figure 2(a)). The Mott transition occurs when the chemical potential reaches the top of the LHB at half-filling before reaching the top of the dispersing mode in the small-doping limit. Although the dispersing mode loses the spectral weight for  $\omega > 0$ , the dispersion relation retains a wide  $\omega$  range even in the small-doping limit [17]. From the insulating side, following the doping of the Mott insulator, a gapless dispersing mode emerges in the Mott gap. The spectral weight of this mode increases as the doping concentration increases [17].

This behavior cannot be explained in the conventional pictures. In the rigid-band picture, the band structure of the Mott insulator is expected to remain unchanged with or without doping (figure 1(a)): the band is simply filled with electrons, and no mode loses the spectral weight. In the electron-like quasiparticle picture, the bandwidth near the Mott transition is expected to become extremely narrow as the effective mass diverges (figure 1(b)): the dispersion relation of the quasiparticle does not retain a wide  $\omega$  range.

In a mean-field (local spin-density) approximation for an antiferromagnetic long-range order, the effective staggered magnetic field causes the energy gap between the UHB and the LHB, and the modes of the single-

particle excitation bend back at the boundaries of the magnetic Brillouin zone even in a doped system (figure 1(a)); the mode exhibiting a free-electron-like dispersion relation is formed by merging the UHB and the LHB when the antiferromagnetic long-range order disappears. However, in the Hubbard model in the large- $U/t$  regime for  $0 < n < 2$ , the UHB is separated from the LHB by an energy gap of  $O(U)$  even without an antiferromagnetic long-range order in the ground state; the free-electron-like mode in a doped system is due to the doping-induced states which gain spectral weights as the doping concentration increases (figure 2(a)).

### 3. Doping-induced states

Although the emergence of states in the Mott gap induced by doping a Mott insulator has been recognized since the early 1990s [13, 33, 34], its interpretations are controversial. Typically, the doping-induced states have been interpreted as

- (i) a part of the UHB, the energy of which is decreased by doping because doping relaxes the binding between double occupancy and vacancy [35];
- (ii) states resulting from the hybridization between composite fermions (cofermions) and the quasi-particles [36, 37];
- (iii) states coupled with the charge- $2e$  boson obtained by integrating the high-energy degrees of freedom [12, 38];
- (iv) a spin-polaron shakeoff band which is disconnected from the low-energy quasiparticle band [39, 40];
- (v) states that lose the spectral weights as the doping concentration decreases and eventually exhibit the momentum-shifted magnetic dispersion relation in the small-doping limit: the mode is gapless in the small-doping limit if the spin excitation is gapless in the Mott insulator [17–23].

These interpretations can be classified in terms of their origin and energy gap. In interpretations (i)–(iii), the doping-induced states are related to double occupancy; the mode of the doping-induced states is separated by an energy gap from the low-energy mode. In interpretations (iv) and (v), although the doping-induced states are related to spin excitation, the mode of the doping-induced states is separated by an energy gap from the low-energy quasiparticle band in (iv) but is gapless in (v) if the spin excitation of the Mott insulator is gapless.

Whether the mode of the doping-induced states is disconnected from the low-energy mode or not

is important not only for the low-energy electronic properties near the Mott transition but also to understand how the free-electron-like electronic state in the large-doping regime changes into the electronic state exhibiting spin-charge separation in the Mott insulator. In (i)–(iv), the mode of the doping-induced states is separated from the low-energy mode by an energy gap, which is considered responsible for the zero surface of the Green function [12, 35–39, 41]. In (v), on the other hand, such an energy gap does not exist in the small-doping limit if the spin excitation of the Mott insulator is gapless; the free-electron-like mode in the large-doping regime can continuously deform into the mode exhibiting the momentum-shifted magnetic dispersion relation in the small-doping limit.

### 4. Relationship between doping-induced states and spin excitation

In the 1D Hubbard model, the properties of the doping-induced states have been clarified using exact solutions and accurate numerical results [17]. Here, to explain the essence, we consider the large- $U/t$  regime.

In the Mott insulator at half-filling, the low-energy properties can be effectively described by the Heisenberg model defined by the following Hamiltonian:

$$\mathcal{H}_{\text{spin}} = J \sum_{\langle i,j \rangle} \mathbf{S}_i \cdot \mathbf{S}_j,$$

where  $\mathbf{S}_i$  denotes the spin operator at site  $i$  and  $J = 4t^2/U$  [27]. The spin-wave dispersion relation is expressed as

$$\omega = v_{1\text{D}} |\sin k|,$$

where  $v_{1\text{D}}$  denotes the spin-wave velocity of the 1D Heisenberg model ( $v_{1\text{D}} = \pi J/2$  [42]). Although low-energy spin excitation exists, there is no electronic state in the Mott gap (figure 2(b)).

On decreasing the chemical potential, the Mott transition occurs when the chemical potential reaches the top of the LHB. Then, infinitesimal doping induces electronic states in the Mott gap (figure 2(a)). The dispersion relation of the doping-induced states in the small-doping limit can essentially be expressed as

$$\omega = -v_{1\text{D}} \cos k$$

for  $\omega > 0$  using the same  $v_{1\text{D}}$  as that of the spin-wave dispersion relation (figure 3(a)) [17]. Thus, the doping-induced states exhibit the spin-wave dispersion relation of the Mott insulator with the momentum shifted by the Fermi momentum ( $\pi/2$ ) in the small-doping limit. The doping-induced states are directly related to the spin excitation and form a gapless mode reflecting the gapless spin excitation of the Mott insulator. As

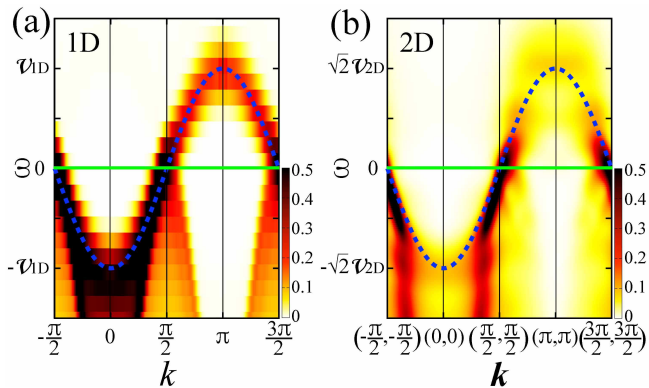


**Figure 3.** Spectral-weight distributions around the Fermi level near the Mott transition in the 1D and 2D Hubbard models for  $U/t = 10$ . (a)  $A(\mathbf{k}, \omega)t$  of the 1D Hubbard model at  $\delta \approx 0.033$ . Close-up of figure 2(a) around the Fermi level [17, 19]. (b)  $A(\mathbf{k}, \omega)t$  of the 2D Hubbard model at  $\delta = 0.04$  obtained using the cluster perturbation theory for  $(4 \times 4)$ -site clusters [18, 19]. The dashed blue curves indicate the spin-wave dispersion relation of the Heisenberg models for  $J = 4t^2/U$ . The spin-wave velocities of the 1D and 2D Heisenberg models are denoted by  $v_{1D}$  and  $v_{2D}$ , respectively. The solid green lines indicate the Fermi level ( $\omega = 0$ ). Gaussian broadening with a standard deviation of 0.1t is used.

the doping concentration increases, the mode of the doping-induced states continuously deforms into the free-electron-like mode in the large-doping regime.

From the metallic side, as the electron density increases, the free-electron-like mode in the large-doping regime continuously deforms, gradually losing the spectral weight for  $\omega > 0$ , and it eventually exhibits the momentum-shifted spin-wave dispersion relation (figure 2(a)). When the chemical potential is increased beyond the top of the LHB at half-filling, the spectral weight of this mode for  $\omega > 0$  disappears completely: the Mott insulating state is realized (figure 2(b)).

Thus, in the 1D Hubbard model, only interpretation (v) among the above interpretations ((i)–(v) in section 3) can account for the behavior of the doping-induced states. The mode of the doping-induced states is gapless and related to the spin excitation of the Mott insulator as well as to the free-electron-like mode in the large-doping regime.

The reason why the momentum is shifted by the Fermi momentum can generally be explained as follows [20]. At half-filling, we assume that (1) the ground state has spin  $S = 0$  and momentum  $\mathbf{k} = \mathbf{0}$ , (2) the spin excitation with  $S = 1$  exhibits the dispersion relation  $\omega = f(\mathbf{k})$ , and (3) the top of the LHB is located at  $\mathbf{k} = -\mathbf{k}_F$  (Fermi momentum in the small-doping limit). When one electron is removed from the Mott insulator, the ground state should have  $S = 1/2$  and  $\mathbf{k} = \mathbf{k}_F$  because the electron having  $S = 1/2$  is removed at  $\mathbf{k} = -\mathbf{k}_F$ . Then, if an electron with momentum  $\mathbf{p}$  is added to the one-hole-doped ground

state, the electronic state has the same number of electrons as that of the Mott insulator,  $S = 0$  or 1 [40], and  $\mathbf{k} = \mathbf{p} + \mathbf{k}_F$  [20]. The state having  $S = 0$  and  $\mathbf{k} = \mathbf{0}$  can have overlap with the ground state of the Mott insulator as in the band insulator case. The state having  $S = 1$  and  $\mathbf{k} = \mathbf{p} + \mathbf{k}_F$  can have overlap with the spin excited state in the Mott insulator at excitation energy  $\omega = f(\mathbf{p} + \mathbf{k}_F)$ ;  $A(\mathbf{k}, \omega)$  shows a mode along  $\omega = f(\mathbf{k} + \mathbf{k}_F)$ . Thus, the doping-induced states in the small-doping limit exhibit the spin-wave dispersion relation shifted by the Fermi momentum [20]. Because this argument relies on neither quasiparticle pictures nor dimensionality, this is a general characteristic of the Mott transition.

The emergence of the spin excited states in the single-particle spectrum along the momentum-shifted dispersion relation at low energies reflects the spin-charge separation of the Mott insulator [20] and contrasts with the band insulator case. In a band insulator, the spin-flip excitation costs energy as large as the band gap because spin-charge separation does not occur. Thus, by doping a band insulator, no state emerges in the band gap. In contrast, in a Mott insulator, there are low-energy spin excited states, which do not appear in the single-particle spectrum, because charge excitation has a much larger energy. By doping a Mott insulator, the electron-addition excited states have overlap not only with the ground state of the Mott insulator but also with the low-energy spin excited states, which leads to the emergence of spectral weights in the single-particle excitation at low energies along the momentum-shifted magnetic dispersion relation in the Mott gap because removing one electron shifts the ground-state momentum by the Fermi momentum.

In the two-dimensional (2D) Hubbard model, essentially the same characteristic has been obtained in a numerical study [18]. Analogously to the above argument for the 1D Hubbard model, we consider the large- $U/t$  regime, assuming that  $U/t$  is not so large as to stabilize ferromagnetic states [43]. In the Mott insulator of the 2D Hubbard model, the low-energy properties are effectively described by the 2D Heisenberg model, which exhibits the spin-wave dispersion relation [44] expressed as

$$\omega = \sqrt{2}v_{2D}|\sin k|$$

for  $\mathbf{k} = (k, k)$  in the  $(0, 0)$ – $(\pi, \pi)$  direction, where  $v_{2D}$  denotes the spin-wave velocity of the 2D Heisenberg model ( $v_{2D} = 1.18(2)\sqrt{2}J$  [45]). In the small-doping regime, the doping-induced states for  $\mathbf{k} = (k, k)$  in the  $(0, 0)$ – $(\pi, \pi)$  direction exhibit the dispersion relation

$$\omega \approx -\sqrt{2}v_{2D}\cos k$$

for  $\omega > 0$  (figure 3(b)), which can essentially be regarded as the magnetic dispersion relation of the

Mott insulator shifted by the Fermi momentum  $\mathbf{k}_F \approx (\pm\pi/2, \pm\pi/2)$  [18]. This is also consistent with the above quantum-number argument.

The reason why almost no spectral weights of the doping-induced states appear in the momentum region inside the Fermi surface in figures 2(a) and 3 is that the LHB in this momentum region is almost completely filled with electrons in the ground state of the doped system [20]: there is almost no room for the added electron inside the Fermi surface in the low-energy regime. As the doping concentration increases, the number of vacancies, which the added electron can enter with energies much smaller than  $U$  in the momentum region outside the Fermi surface, increases. Thus, increasing the spectral weights in the low-energy regime outside the Fermi surface, the mode of the doping-induced states deforms into the free-electron-like mode carrying considerable spectral weights in the large-doping regime.

As mentioned in section 3, there have also been numerical or approximate results from which other interpretations have been derived for 2D Hubbard-type models ((i)–(iv) in section 3) [12, 35–41].

In the following, we consider how the characteristics of the electronic state near the Mott transition are related to the anomalous features observed in high- $T_c$  cuprates [5–13].

### 5. Anomalous spectral features observed in high-temperature cuprate superconductors

High- $T_c$  cuprates exhibit superconductivity at much higher temperatures (the maximum value of the transition temperature  $T_c$  observed so far is approximately 133 K at ambient pressure [46]) compared to conventional superconductors (the values of  $T_c$  of conventional superconductors are typically less than 40 K at ambient pressure). The anomalously high value of  $T_c$  is considered to be due to the anomalous electronic states of high- $T_c$  cuprates, which are obtained by doping Mott insulators. Thus, the understanding of the electronic states near the Mott transition is considered key to revealing the mechanism of high- $T_c$  superconductivity [13–16].

The following are typical anomalous features of electronic states observed in high- $T_c$  cuprates:

- (a) *Doping-induced states*.—Spectral weights are induced in the Mott gap by doping Mott insulators [7, 12].
- (b) *Spinon-like branch and holon-like branch*.—The dispersion relation below the Fermi level in hole-doped systems shows two branches similar to the spinon and holon modes of 1D systems [6].
- (c) *Giant kink and waterfall*.—The dispersion relation below the Fermi level in hole-doped systems

exhibits a kink. The dispersion relation becomes steeper, and the spectral weights are significantly reduced immediately below the kink [6].

- (d) *Flat band*.—The dominant mode around  $\mathbf{k} \approx (\pm\pi, 0)$  and  $(0, \pm\pi)$  exhibits a flat dispersion relation in a wide momentum region below the Fermi level near the Mott transition in hole-doped systems [8, 9].
- (e) *Pseudogap*.—The spectral weight is reduced near the Fermi level [5, 13, 15].
- (f) *Fermi arc*.—The spectral weights of some parts of the Fermi surface are significantly reduced near the Mott transition. In hole-doped systems, spectral weights near the Fermi level are primarily located only around  $(\pm\pi/2, \pm\pi/2)$  [9, 10]. In contrast, those in electron-doped systems are primarily located only around  $(\pm\pi, 0)$  and  $(0, \pm\pi)$  [11].

### 6. Single-particle spectral properties of the two-dimensional Hubbard model

We interpret the above anomalous features from the viewpoint of the proximity of the Mott transition based on recent results for 2D Hubbard models [18, 24]. Without loss of generality, we primarily consider the properties for  $0 \leq k_y \leq k_x \leq \pi$  on a square lattice. In this section, we consider the hole-doped case of the 2D Hubbard model; the spectral function in the electron-doped case can be obtained by reversing the spectral function in the hole-doped case with respect to  $\omega = 0$  and  $\mathbf{k} = (\pi/2, \pi/2)$  in the 2D Hubbard model.

#### 6.1. Properties along $(0, 0) - (\pi, \pi)$

We first consider the spectral properties along  $(0, 0) - (\pi, \pi)$ . As discussed in section 4, the low-energy spin excited states of the Mott insulator generally emerge in the electron-addition spectrum ( $\omega > 0$ ) on doping a Mott insulator, and the spectral weight increases as the doping concentration increases. Thus, the doping-induced spectral weights observed in high- $T_c$  cuprates ((a) in section 5) [7] can be interpreted as the doping-induced states characteristic of the Mott transition (figure 3(b); I in figure 4(c)).

We turn our attention to the spectral properties for the electron-removal excitation ( $\omega < 0$ ). In 1D systems, the electron-removal excitation primarily exhibits two modes: the spinon and holon modes (figure 5(a)) [17, 31, 32], which primarily reflect the spin and charge degrees of freedom, respectively. The bandwidths of the spinon and holon modes are essentially proportional to the spin exchange coupling  $J$  and the hopping integral  $t$ , respectively; the former is about the value of the spin-wave velocity ( $\approx \pi J/2$ ),



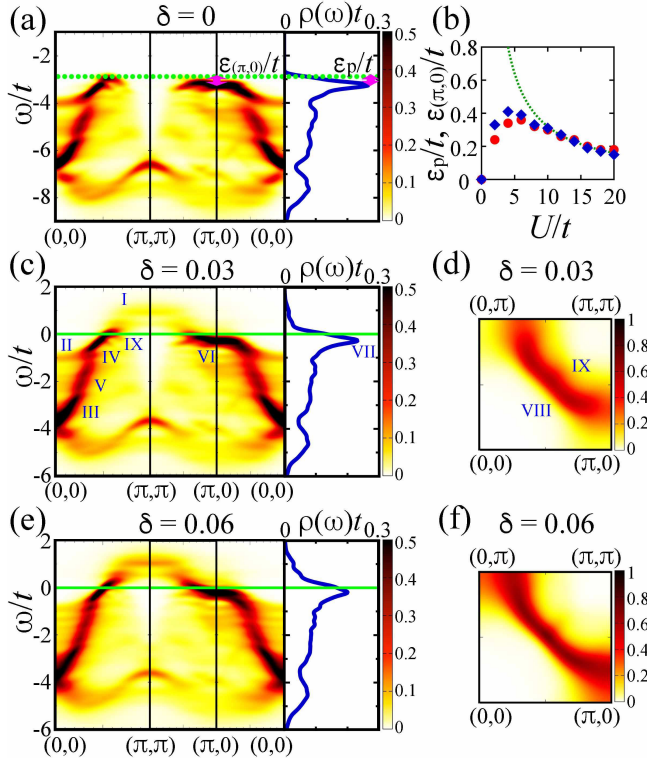


**Figure 4.** Spectral-weight distributions in the LHB of the 2D Hubbard model for  $U/t = 10$  obtained using the cluster perturbation theory for  $(4 \times 4)$ -site clusters [18]. (a)  $A(\mathbf{k}, \omega)t$  at  $\delta = 0$ . The dotted green line indicates the top of the LHB. The pseudogap defined by the flat mode at  $(\pi, 0)$  and that by the main peak of  $\rho(\omega)$  are denoted by  $\varepsilon_{(\pi,0)}$  and  $\varepsilon_p$ , respectively. (b)  $\varepsilon_p/t$  (blue diamonds) and  $\varepsilon_{(\pi,0)}/t$  (red circles), taken from Ref. [18]. The dotted green curve indicates a fit in the large- $U/t$  regime, assuming  $\varepsilon_p, \varepsilon_{(\pi,0)} \propto J (= 4t^2/U)$ . (c)  $A(\mathbf{k}, \omega)t$  at  $\delta = 0.03$ . (d)  $A(\mathbf{k}, \omega \approx 0)t$  at  $\delta = 0.03$ . In (c) and (d), I–IX denote spectral features. I: doping-induced states, II: spinon-like branch, III: holon-like branch, IV: giant kink, V: waterfall, VI: flat mode, VII: pseudogap, VIII: Fermi arc, and IX: hole-pocket-like behavior. (e)  $A(\mathbf{k}, \omega)t$  at  $\delta = 0.06$ . (f)  $A(\mathbf{k}, \omega \approx 0)t$  at  $\delta = 0.06$ . In (a), (c), and (e), the rightmost panels show  $\rho(\omega)t (\equiv \int d\mathbf{k} A(\mathbf{k}, \omega)t / (2\pi)^2)$ . The solid green lines in (c) and (e) indicate the Fermi level ( $\omega = 0$ ). Gaussian broadening with a standard deviation of  $0.1t$  is used in (a) and (c)–(f).

and the latter, defined by  $|\omega|$  at  $k = 0$ , is approximately  $2t$  near the Mott transition.

This feature is modified by introducing interchain hopping. If the interchain hopping integral  $t_\perp (> 0)$  is small, its effects can be investigated using the perturbation theory. By assuming that the chains are aligned in the  $x$ -direction and that they are coupled in the  $y$ -direction, the inverse of the single-particle Green function can be approximated up to the first order in  $t_\perp$  [47, 48] as

$$G^{-1}(\mathbf{k}, \omega) \approx G_{1D}^{-1}(k_x, \omega) - t_\perp(k_y),$$

where  $G_{1D}(k_x, \omega)$  denotes the Green function of a 1D chain and  $t_\perp(k_y) = -2t_\perp \cos k_y$ . In this approximation, which is called the random-phase

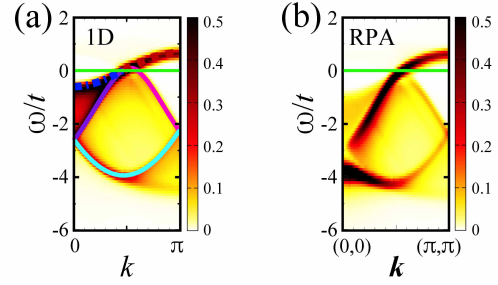


**Figure 5.** Dominant modes of the 1D Hubbard model and their shift by interchain hopping. (a)  $A(\mathbf{k}, \omega)t$  in the LHB of the 1D Hubbard model for  $U/t = 10$  at  $\delta \approx 0.067$  obtained using the non-Abelian DDMRG method on a 120-site chain with 120 density-matrix eigenstates [17, 21]. The dashed red curve for  $\omega > 0$  indicates the upper edge of the spinon-antiholon continuum, which corresponds to the doping-induced states. The dash-dotted blue curve indicates the spinon mode. The solid curves indicate the holon ( $\omega < 0$ ) and antiholon ( $\omega > 0$ ) modes. (b)  $A(\mathbf{k}, \omega)t$  along  $(0, 0)$ – $(\pi, \pi)$  obtained by the RPA for interchain hopping ( $t_\perp = t$ ) using the data in (a) [18]. The solid green lines at  $\omega = 0$  indicate the Fermi level. Gaussian broadening with a standard deviation of  $0.1t$  is used.

approximation (RPA), the spectral weights are shifted to lower (higher) values of  $\omega$  in the momentum region of  $t_\perp(k_y) < 0$  ( $t_\perp(k_y) > 0$ ) by interchain hopping; the shift becomes large for modes carrying large spectral weights [49, 50].

From this viewpoint, we can infer how the spectral weights shift as interchain hopping is introduced near the Mott transition (figure 5(b)) [18]. Around  $(0, 0)$ , spectral weights are expected to shift significantly to lower values of  $\omega$  because there are considerable spectral weights around  $k_x \approx 0$  in the LHB of the 1D Hubbard model (figure 5(a)) and because  $t_\perp(k_y \approx 0) \approx -2t_\perp < 0$ . On the other hand, around  $(\pi, \pi)$ , we expect that spectral weights shift to higher values of  $\omega$  because  $t_\perp(k_y \approx \pi) \approx 2t_\perp > 0$ , but the shift would be small because the spectral weights are relatively small around  $k_x \approx \pi$  in the LHB of the 1D Hubbard model (figure 5(a)). Around  $(\pi/2, \pi/2)$ , we expect that spectral weights remain almost unaffected by the interchain hopping because  $t_\perp(k_y \approx \pi/2) \approx 0$ .

The overall behavior of the spectral-weight distribution of the 2D Hubbard model can be interpreted basically from this viewpoint [18]. There are two branches around  $(0, 0)$  for  $\omega < 0$ : the higher- $\omega$  and lower- $\omega$  branches can be interpreted as those originating primarily from the spinon and holon modes, respectively (II and III in figure 4(c)). They are shifted to lower values of  $\omega$  from the corresponding 1D modes because of the interchain hopping ( $t_\perp(k_y \approx 0) < 0$ ). At the bifurcation point of these two branches, the dispersion relation exhibits a kink (IV in figure 4(c)) because their bandwidths are different: the bandwidth of the higher- $\omega$  branch ( $\approx \sqrt{2}v_{2D}$ ; figure 3(b)) is primarily determined by the spin-

wave velocity, whereas the bandwidth of the lower- $\omega$  branch ( $\approx 4t$ ) is primarily determined by the hopping integral. Although the RPA is too simple to explain the reduction in spectral weight immediately below the kink, the numerical results for the 2D Hubbard model obtained using the cluster perturbation theory, in which fluctuations within clusters are treated exactly [51,52], show behavior similar to the waterfall behavior observed in high- $T_c$  cuprates (V in figure 4(c)) [18]. Thus, the spinon-like branch, holon-like branch, giant kink, and waterfall behavior observed in high- $T_c$  cuprates ((b) and (c) in section 5) can be accounted for as properties of a 2D system near the Mott transition.

The branches responsible for the giant kink and waterfall behavior have also been interpreted as the low- $|\omega|$  renormalized quasiparticle band and the high- $|\omega|$  damped spin fluctuation continuum [53], string-like excitations [54], or an incoherent band [55]. Moreover, there have been interpretations based on composite-field pictures [12,56].

From the viewpoint of the weakly coupled chains, we expect that the properties around  $(\pi/2, \pi/2)$  remain almost unaffected by the interchain hopping. This suggests that hole-pocket-like behavior persists around  $(\pi/2, \pi/2)$ : the mode originating from the holon and antiholon modes is expected to bend back around  $(\pi/2, \pi/2)$  (IX in figures 4(c) and 4(d)). However, the spectral weights around the Fermi level outside the Fermi surface would become very small as the doping concentration increases.

## 6.2. Properties around $(\pi, 0)$

We next consider the spectral properties around  $(\pi, 0)$ . In this momentum region, the flat mode carrying large spectral weights is dominant [13], and it is located slightly below the Fermi level near the Mott transition (VI in figure 4(c)) [18, 57, 58]. In the noninteracting case ( $U = 0$ ), this mode causes the Van Hove singularity at the Fermi level at half-filling. When the interaction is turned on, the Mott gap opens, and the mode around  $(\pi, 0)$  becomes flat in a wider momentum region ((d) in section 5). Because the top of the LHB at half-filling is located near  $(\pi/2, \pi/2)$  (figure 4(a)), this mode is located slightly below the Fermi level near the Mott transition. Because this flat mode carries large spectral weights, it substantially contributes to the main peak of the single-particle density of states. The existence of the flat mode slightly below the Fermi level near the Mott transition implies that the density of states is relatively reduced near the Fermi level (VII in figure 4(c)) [18]. This behavior is referred to as a pseudogap ((e) in section 5). Although there are several kinds of pseudogaps observed in high- $T_c$  cuprates [5, 13, 15], here, we consider the pseudogap defined by the main peak of the single-particle density

of states to discuss the overall spectral feature. The pseudogap energy is defined by  $|\omega|$  of the main peak of the density of states, which is essentially the same as  $|\omega|$  of the flat mode around  $(\pi, 0)$  in the small-doping limit (figure 4(b)). The numerical results indicate that the pseudogap energy is almost proportion to  $J(= 4t^2/U)$  in the large- $U/t$  regime (figure 4(b)), which implies that it is related to the antiferromagnetic fluctuation [18, 58]. As the electron density (or the chemical potential) decreases, the pseudogap decreases (figure 4(e)) and closes at a  $\delta$  value where the main peak of the density of states or the flat mode around  $(\pi, 0)$  crosses  $\omega = 0$ .

Because the flat mode is located around  $(\pi, 0)$  below the Fermi level near the Mott transition, there is no mode crossing the Fermi level along  $(0, 0) - (\pi, 0)$  (figures 4(c) and 4(d)). In addition, the spectral weights along  $(\pi, 0) - (\pi, \pi)$  near the Fermi level should be significantly reduced because the spectral weights disappear toward the Mott transition. Thus, the spectral weights near the Fermi level primarily remain only around  $(\pi/2, \pi/2)$  near the Mott transition. This feature is referred to as Fermi arc behavior (VIII in figure 4(d); (f) in section 5). Accordingly, the Fermi arc behavior can be explained as a consequence of the shift of the flat mode below the Fermi level and the reduction in spectral weight of the mode crossing the Fermi level near the Mott transition [18]. As the doping concentration increases, the portion of the Fermi surface having a large spectral weight becomes longer (figure 4(f)), which leads to the free-electron-like Fermi surface in the large-doping regime.

## 7. Effects of next-nearest-neighbor hopping

To account for the asymmetry of electronic states between hole-doped and electron-doped high- $T_c$  cuprates [5, 11], we consider the effects of next-nearest-neighbor hopping. The next-nearest-neighbor hopping term is defined by

$$\mathcal{H}_{\text{nnn}} = t' \sum_{\langle\langle i, j \rangle\rangle, \sigma} (c_{i, \sigma}^\dagger c_{j, \sigma} + \text{H.c.}),$$

where  $\langle\langle i, j \rangle\rangle$  indicates that  $i$  and  $j$  are next-nearest-neighbor sites. The numerical results for the 2D Hubbard model with next-nearest-neighbor hopping are shown in figure 6. At half-filling, the spectral-weight distribution becomes asymmetric between the LHB and the UHB because of the  $t'$  term (figure 6(a)). In particular, the bottom of the UHB is located near  $(\pi, 0)$  for moderate values of  $t' (\approx 0.3t)$ , whereas the top of the LHB remains near  $(\pi/2, \pi/2)$ , which causes significant difference in the Fermi surface in the small-doping regime: electrons primarily enter the momentum region around  $(\pi, 0)$  in the electron-doped



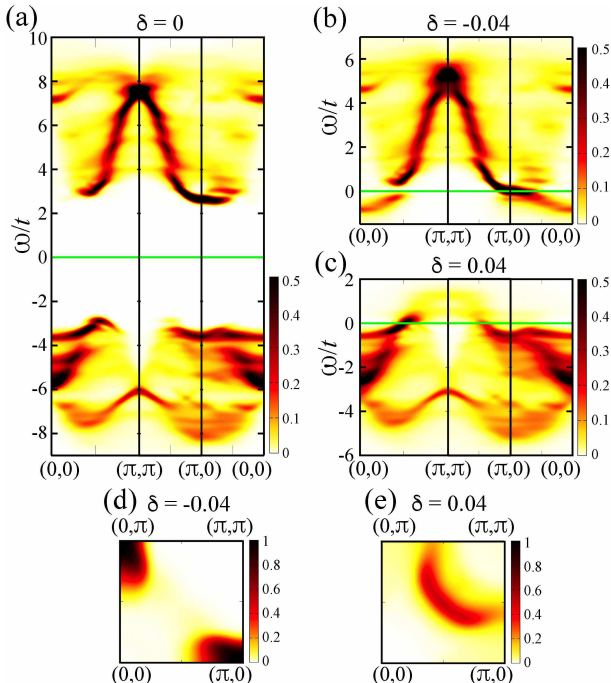


**Figure 6.** Spectral-weight distributions of the 2D Hubbard model with next-nearest-neighbor hopping for  $U/t = 10$  and  $t'/t = 0.3$  obtained using the cluster perturbation theory for  $(4 \times 4)$ -site clusters [24]. (a)  $A(\mathbf{k}, \omega)t$  at  $\delta = 0$ . (b)  $A(\mathbf{k}, \omega)t$  in the UHB at  $\delta = -0.04$ . (c)  $A(\mathbf{k}, \omega)t$  in the LHB at  $\delta = 0.04$ . (d)  $A(\mathbf{k}, \omega \approx 0)t$  at  $\delta = -0.04$ . (e)  $A(\mathbf{k}, \omega \approx 0)t$  at  $\delta = 0.04$ . The green lines in (a)–(c) indicate the Fermi level ( $\omega = 0$ ). Gaussian broadening with a standard deviation of  $0.1t$  is used.

case, whereas holes primarily enter the momentum region around  $(\pi/2, \pi/2)$  in the hole-doped case (figures 6(b)–6(e)). This feature has been observed in numerical calculations for Hubbard-type models with next-nearest-neighbor hopping [24, 25, 41, 52, 59–66] and in experiments for high- $T_c$  cuprates [9–11].

The effects of the  $t'$  term on the overall spectral features can be interpreted using the RPA-type approximation [24]. Analogously to the RPA for interchain hopping (section 6.1), the inverse of the single-particle Green function is approximated as

$$G^{-1}(\mathbf{k}, \omega) \approx G_{2D}^{-1}(\mathbf{k}, \omega) - t'(\mathbf{k}),$$

where  $G_{2D}(\mathbf{k}, \omega)$  denotes the Green function of the 2D Hubbard model without next-nearest-neighbor hopping and  $t'(\mathbf{k}) = 4t' \cos k_x \cos k_y$ . In this approximation [24], the spectral weights are shifted to lower (higher) values of  $\omega$  in the momentum region of  $t'(\mathbf{k}) < 0$  ( $t'(\mathbf{k}) > 0$ ) by next-nearest-neighbor hopping, and the shift becomes large for modes carrying large spectral weights, as in the RPA for interchain hopping (section 6.1).

According to this argument, the spectral weights around  $(0, 0)$  and  $(\pi, \pi)$  are shifted to higher values of  $\omega$ , whereas those around  $(\pi, 0)$  are shifted to lower

values of  $\omega$  particularly for modes carrying large spectral weights. Thus, the Fermi-arc behavior and pseudogap behavior caused by the flat mode around  $(\pi, 0)$  are enhanced in the hole-doped case (figures 6(c) and 6(e)). In contrast, in the electron-doped case for moderate values of  $t'(\approx 0.3t)$ , because the flat mode around  $(\pi, 0)$  is shifted by next-nearest-neighbor hopping to lower values of  $\omega$  than the bottom of the UHB of the 2D Hubbard model at half-filling around  $(\pi/2, \pi/2)$ , considerable spectral weights are located around  $(\pi, 0)$  near the Fermi level near the Mott transition (figures 6(b) and 6(d)) ((f) in section 5) [24]. In this interpretation, it is not necessary to assume antiferromagnetic long-range order in hole-doped and electron-doped systems, and the characteristic electronic states near the Mott transition, such as the doping-induced states, can collectively be explained as shifted states from those of the 2D Hubbard model (section 6; figure 4) by next-nearest-neighbor hopping [24].

As for the electronic states near the Mott transition in electron-doped systems, there have also been interpretations based on antiferromagnetic long-range order [67, 68].

## 8. Discussion and summary

In this paper, a new picture of the Mott transition regarding how electrons behaving as single particles in a metal change into those exhibiting the spin-charge separation of the Mott insulator was presented [17–23]. The Mott transition is characterized as the freezing of the charge degrees of freedom while the spin degrees of freedom remain active: the mode of the electron-addition excitation in the LHB loses the spectral weight while the dispersion relation deforms into the momentum-shifted magnetic dispersion relation of the Mott insulator. This is also reasonable in view of the fact that the Mott transition is caused by the Coulomb repulsion, i.e., repulsive interaction between charges. From the insulating side, this characteristic can be described as the emergence of spin excitation in the electron-addition spectrum with the dispersion relation shifted by the Fermi momentum because the charge character is added by doping. Because the dispersion relation of the doping-induced states is shifted from that of the spin excitation by the Fermi momentum, the mode of the doping-induced states can be gapless if the spin excitation is gapless. As the doping concentration increases, this mode deforms into the free-electron-like mode in the large-doping regime, increasing the spectral weight. This characteristic of the Mott transition reflects the spin-charge separation (existence of low-energy spin excitation despite a large charge gap) in a Mott insulator. The rigid-band picture

and the electron-like quasiparticle picture cannot explain this characteristic because these conventional pictures do not properly describe the spin-charge separation of the Mott insulator.

This characteristic of the Mott transition is relevant to spectral features observed in high- $T_c$  cuprates; the reduction in spectral weight is related to the doping-induced states and to the Fermi arc. The strong low-energy spin fluctuation near the Mott transition is related to the bifurcation of the mode of single-particle excitation into the spinon-like branch and holon-like branch, which causes the giant kink and waterfall behavior. The pseudogap and the flat mode around  $(\pi, 0)$  are also related to the antiferromagnetic fluctuation, because their energies are almost proportional to  $J(= 4t^2/U)$  in the large- $U/t$  regime in the 2D Hubbard model. Thus, various spectral features observed in high- $T_c$  cuprates, which seemed to be anomalous in conventional pictures, are explained as properties of a 2D system near the Mott transition [18].

The asymmetric spectral-weight distribution between hole-doped and electron-doped systems can be explained by considering how the spectral-weight distribution of the 2D Hubbard model is shifted by next-nearest-neighbor hopping [24]. The spectral-weight distribution along  $(0, 0) - (\pi, \pi)$  in the 2D Hubbard model can further be explained by considering how interchain hopping modifies the spectral-weight distribution of the 1D Hubbard model [17, 18]. Thus, the overall spectral features of 2D systems near the Mott transition can be interpreted by tracing the origins to those of 1D systems.

Because essentially the same spectral features have been obtained in the  $t$ - $J$  models [20–22, 25], the spectral features discussed in this paper are not specific to the Hubbard models. The existence of double occupancy is not essential for these features, because double occupancy does not exist in the  $t$ - $J$  models.

To clarify properties in the very small- $|\omega|$  regime near the Mott transition, further studies are necessary; the possibility of  $d$ -wave superconductivity or antiferromagnetic long-range order in the ground state of 2D Hubbard-type models is not ruled out.

In this paper, overall spectral features near the filling-controlled continuous Mott transition were discussed to clarify the nature of the Mott transition. In real materials, Mott transitions can be of the first order because of effects that were not considered in this paper. Furthermore, the ground state near the Mott transition can be a  $d$ -wave superconducting state or an antiferromagnetically ordered state. Nevertheless, signatures of the overall spectral features near the Mott transition discussed in this paper would generally appear primarily at energies of  $O(J)$ , as observed

in high- $T_c$  cuprates. In particular, the emergence of electronic states exhibiting the momentum-shifted magnetic dispersion relation following doping, which reflects the spin-charge separation of a Mott insulator, is a general and fundamental characteristic of the Mott transition that is elusive in conventional single-particle pictures.

## Acknowledgments

This work was supported by JSPS KAKENHI Grant Numbers 23540428 and 26400372, and the World Premier International Research Center Initiative (WPI), MEXT, Japan.

## References

- [1] Ashcroft N W and Mermin N D 1976 *Solid State Physics* (Cengage Learning, Boston, United States)
- [2] Mott N F 1949 The basis of the electron theory of metals, with special reference to the transition metals *Proc. Phys. Soc. A* **62** 416–22
- [3] Imada M, Fujimori A and Tokura Y 1998 Metal-insulator transitions *Rev. Mod. Phys.* **70** 1039–263
- [4] Bednorz J G and Müller K A 1986 Possible high  $T_c$  superconductivity in the Ba–La–Cu–O system *Z. Phys. B* **64** 189–93
- [5] Damascelli A, Hussain Z and Shen Z-X 2003 Angle-resolved photoemission studies of the cuprate superconductors *Rev. Mod. Phys.* **75** 473–541
- [6] Graf J, Gweon G-H, McElroy K, Zhou S Y, Jozwiak C, Rotenberg E, Bill A, Sasagawa T, Eisaki H, Uchida S, Takagi H, Lee D-H and Lanzara A 2007 Universal high energy anomaly in the angle-resolved photoemission spectra of high temperature superconductors: possible evidence of spinon and holon branches *Phys. Rev. Lett.* **98** 067004
- [7] Chen C T, Sette F, Ma Y, Hybertsen M S, Stechel E B, Foulkes W M C, Schluter M, Cheong S-W, Cooper A S, Rupp L W, Batlogg B, Soo Y L, Ming Z H, Krol A and Kao Y H 1991 Electronic states in  $\text{La}_{2-x}\text{Sr}_x\text{CuO}_{4+\delta}$  probed by soft-X-ray absorption *Phys. Rev. Lett.* **66** 104–7
- [8] Dessau D S, Shen Z-X, King D M, Marshall D S, Lombardo L W, Dickinson P H, Loeser A G, DiCarlo J, Park C-H, Kapitulnik A and Spicer W E 1993 Key features in the measured band structure of  $\text{Bi}_2\text{Sr}_2\text{CaCu}_2\text{O}_{8+\delta}$ : Flat bands at  $E_F$  and Fermi surface nesting *Phys. Rev. Lett.* **71** 2781–4
- [9] Marshall D S, Dessau D S, Loeser A G, Park C-H, Matsuura A Y, Eckstein J N, Bozovic I, Fournier P, Kapitulnik A, Spicer W E and Shen Z-X 1996 Unconventional electronic structure evolution with hole doping in  $\text{Bi}_2\text{Sr}_2\text{CaCu}_2\text{O}_{8+\delta}$ : Angle-resolved photoemission results *Phys. Rev. Lett.* **76** 4841–4
- [10] Yoshida T, Zhou X J, Tanaka K, Yang W L, Hussain Z, Shen Z-X, Fujimori A, Sahrakorpi S, Lindroos M, Markiewicz R S, Bansil A, Komiya S, Ando Y, Eisaki H, Kakeshita T and Uchida S 2006 Systematic doping evolution of the underlying Fermi surface of  $\text{La}_{2-x}\text{Sr}_x\text{CuO}_4$  *Phys. Rev. B* **74** 224510
- [11] Armitage N P, Fournier P and Greene R L 2010 Progress and perspectives on electron-doped cuprates *Rev. Mod. Phys.* **82** 2421–87

- [12] Phillips P, Choy T-P and Leigh R G 2009 Mottness in high-temperature copper-oxide superconductors *Rep. Prog. Phys.* **72** 036501
- [13] Dagotto E 1994 Correlated electrons in high-temperature superconductors *Rev. Mod. Phys.* **66** 763–840
- [14] Anderson P W 1987 The resonating valence bond state in  $\text{La}_2\text{CuO}_4$  and superconductivity *Science* **235** 1196–8
- [15] Lee P A, Nagaosa N and Wen X-G 2006 Doping a Mott insulator: Physics of high-temperature superconductivity *Rev. Mod. Phys.* **78** 17–85
- [16] Ogata M and Fukuyama H 2008 The  $t$ - $J$  model for the oxide high- $T_c$  superconductors *Rep. Prog. Phys.* **71** 036501
- [17] Kohno M 2010 Spectral properties near the Mott transition in the one-dimensional Hubbard model *Phys. Rev. Lett.* **105** 106402
- [18] Kohno M 2012 Mott transition in the two-dimensional Hubbard model *Phys. Rev. Lett.* **108** 076401
- [19] Kohno M 2014 Relationship between single-particle excitation and spin excitation at the Mott transition *JPS Conf. Proc.* **3** 013020
- [20] Kohno M 2015 States induced in the single-particle spectrum by doping a Mott insulator *Phys. Rev. B* **92** 085129
- [21] Kohno M 2015 Spectral properties near the Mott transition in the two-dimensional  $t$ - $J$  model *Phys. Rev. B* **92** 085128
- [22] Kohno M 2015 Doping-induced states in the single-particle spectrum originating from magnetic excitation of a Mott insulator *Phys. Procedia* **75** 206–13
- [23] Kohno M 2016 Mott transition and electronic states of high-temperature superconductors—New development from the Hubbard model *Butsuri* **71** 533–40
- [24] Kohno M 2014 Spectral properties near the Mott transition in the two-dimensional Hubbard model with next-nearest-neighbor hopping *Phys. Rev. B* **90** 035111
- [25] Kohno M 2017 Spectral properties near the Mott transition in the two-dimensional  $t$ - $J$  model with next-nearest-neighbor hopping *Physica B* 10.1016/j.physb.2017.09.084
- [26] Hubbard J 1963 Electron correlations in narrow energy bands *Proc. R. Soc. Lond. A* **276** 238–57
- [27] Anderson P W 1959 New approach to the theory of superexchange interactions *Phys. Rev.* **115** 2–13
- [28] Lieb E H and Wu F Y 1968 Absence of Mott transition in an exact solution of the short-range, one-band model in one dimension *Phys. Rev. Lett.* **20** 1445–8
- [29] Takahashi M 1999 *Thermodynamics of One-Dimensional Solvable Models* (Cambridge University Press, Cambridge, United Kingdom)
- [30] Essler F H L, Frahm H, Göhmann F, Klümper A and Korepin V E 2005 *The One-Dimensional Hubbard Model* (Cambridge University Press, Cambridge, United Kingdom)
- [31] Schulz H J 1993 *Correlated Electron Systems*, edited by V. J. Emery (World Scientific, Singapore) 199–241
- [32] Benthien H, Gebhard F and Jeckelmann E 2004 Spectral function of the one-dimensional Hubbard model away from half filling *Phys. Rev. Lett.* **92** 256401
- [33] Eskes H, Meinders M B J and Sawatzky G A 1991 Anomalous transfer of spectral weight in doped strongly correlated systems *Phys. Rev. Lett.* **67** 1035–8
- [34] Dagotto E, Moreo A, Ortolani F, Riera J and Scalapino D J 1991 Density of states of doped Hubbard clusters *Phys. Rev. Lett.* **67** 1918–21
- [35] Sakai S, Motome Y and Imada M 2009 Evolution of electronic structure of doped Mott insulators: Reconstruction of poles and zeros of Green's function *Phys. Rev. Lett.* **102** 056404
- [36] Yamaji Y and Imada M 2011 Composite-fermion theory for pseudogap, Fermi arc, hole pocket, and non-Fermi liquid of underdoped cuprate superconductors *Phys. Rev. Lett.* **106** 016404
- [37] Yamaji Y and Imada M 2011 Composite fermion theory for pseudogap phenomena and superconductivity in underdoped cuprate superconductors *Phys. Rev. B* **83** 214522
- [38] Phillips P 2010 Colloquium: Identifying the propagating charge modes in doped Mott insulators *Rev. Mod. Phys.* **82** 1719–42
- [39] Eder R, Seki K and Ohta Y 2011 Self-energy and Fermi surface of the two-dimensional Hubbard model *Phys. Rev. B* **83** 205137
- [40] Eder R and Ohta Y 1996 Inverse photoemission in strongly correlated electron systems *Phys. Rev. B* **54** 3576–9
- [41] Sakai S, Motome Y and Imada M 2010 Doped high- $T_c$  cuprate superconductors elucidated in the light of zeros and poles of the electronic Green's function *Phys. Rev. B* **82** 134505
- [42] des Cloizeaux J and Pearson J J 1962 Spin-wave spectrum of the antiferromagnetic linear chain *Phys. Rev.* **128** 2131–5
- [43] Nagaoka Y 1966 Ferromagnetism in a narrow, almost half-filled  $s$  band *Phys. Rev.* **147** 392–405
- [44] Anderson P W 1952 An approximate quantum theory of the antiferromagnetic ground state *Phys. Rev.* **86** 694–701
- [45] Singh R R P and Huse D A 1989 Microscopic calculation of the spin-stiffness constant for the spin-1/2 square-lattice Heisenberg antiferromagnet *Phys. Rev. B* **40** 7247–51
- [46] Schilling A, Cantoni M, Guo J D and Ott H R 1993 Superconductivity above 130 K in the Hg–Ba–Ca–Cu–O system *Nature* **363** 56–8
- [47] Wen X G 1990 Metallic non-Fermi-liquid fixed point in two and higher dimensions *Phys. Rev. B* **42** 6623–30
- [48] Arrighoni E 1998 Interchain coherence of coupled Luttinger liquids at all orders in perturbation theory *Phys. Rev. Lett.* **80** 790–3
- [49] Kohno M, Starykh O A and Balents L 2007 Spinons and triplons in spatially anisotropic frustrated antiferromagnets *Nat. Phys.* **3** 790–5
- [50] Kohno M 2009 Quasiparticles of spatially anisotropic triangular antiferromagnets in a magnetic field *Phys. Rev. Lett.* **103** 197203
- [51] Sénéchal D, Perez D and Pioro-Ladrière M 2000 Spectral weight of the Hubbard model through cluster perturbation theory *Phys. Rev. Lett.* **84** 522–5
- [52] Sénéchal D, Perez D and Plouffe D 2002 Cluster perturbation theory for Hubbard models *Phys. Rev. B* **66** 075129
- [53] Macridin A, Jarrell M, Maier T and Scalapino D J 2007 High-energy kink in the single-particle spectra of the two-dimensional Hubbard model *Phys. Rev. Lett.* **99** 237001
- [54] Manousakis E 2007 String excitations of a hole in a quantum antiferromagnet and photoelectron spectroscopy *Phys. Rev. B* **75** 035106
- [55] Zemljič M M, Prelovšek P and Tohyama T 2008 Temperature and doping dependence of the high-energy kink in cuprates *Phys. Rev. Lett.* **100** 036402
- [56] Avella A 2014 Composite Operator Method Analysis of the Underdoped Cuprates Puzzle *Adv. Cond. Matt. Phys.* **2014** 515698
- [57] Bulut N, Scalapino D J and White S R 1994 Quasiparticle dispersion in the cuprate superconductors and the two-dimensional Hubbard model *Phys. Rev. B* **50** 7215–8
- [58] Preuss R, Hanke W, Gröber C and Evertz H G 1997 Pseudogaps and their Interplay with Magnetic Excitations in the doped 2D Hubbard Model *Phys. Rev. Lett.* **79** 1122–5
- [59] Tohyama T and Maekawa S 2001 Electronic states in the antiferromagnetic phase of electron-doped high- $T_c$  cuprates *Phys. Rev. B* **64** 212505
- [60] Tohyama T 2004 Asymmetry of the electronic states in hole- and electron-doped cuprates: Exact diagonalization

- study of the  $t-t'-t''-J$  model *Phys. Rev. B* **70** 174517
- [61] Sénéchal D and Tremblay A-M S 2004 Hot spots and pseudogaps for hole- and electron-doped high-temperature superconductors *Phys. Rev. Lett.* **92** 126401
- [62] Civelli M, Capone M, Kancharla S S, Parcollet O and Kotliar G 2005 Dynamical breakup of the Fermi surface in a doped Mott insulator *Phys. Rev. Lett.* **95** 106402
- [63] Dahnken C, Potthoff M, Arrigoni E and Hanke W 2006 Correlated band structure of electron-doped cuprate materials *Low Temp. Phys.* **32** 457–61
- [64] Macridin A, Jarrell M, Maier T, Kent P R C and D'Azevedo E 2006 Pseudogap and antiferromagnetic correlations in the Hubbard model *Phys. Rev. Lett.* **97** 036401
- [65] Kyung B, Kancharla S S, Sénéchal D, Tremblay A-M S, Civelli M and Kotliar G 2006 Pseudogap induced by short-range spin correlations in a doped Mott insulator *Phys. Rev. B* **73** 165114
- [66] Zemljic M M, Prelovšek P and Tohyama T 2007 Fermi surface and pseudogap of electron-doped cuprate superconductors: Numerical study of the  $t-t'-J$  model *Phys. Rev. B* **76** 012502
- [67] Kusko C, Markiewicz R S, Lindroos M and Bansil A 2002 Fermi surface evolution and collapse of the Mott pseudogap in  $\text{Nd}_{2-x}\text{Ce}_x\text{CuO}_{4\pm\delta}$  *Phys. Rev. B* **66** 140513
- [68] Kusunose H and Rice T M 2003 Single-particle spectrum in the electron-doped cuprates *Phys. Rev. Lett.* **91** 186407